Current Research in Food Science 5 (2022) 964–972

Contents lists available at ScienceDirect

Current Research in Food Science

journal homepage: www.sciencedirect.com/journal/current-research-in-food-science

Ultrasound-assisted pH-shifting remodels egg-yolk low-density lipoprotein to enable construction of a stable aqueous solution of vitamin D_3

Haolong Ye [a,1], Jinqiu Wang [a,1], Ning Wang [b], Di Wu [a], Hanmei Li [a], Fang Geng [a,*]

[a] Institute for Egg Science and Technology, School of Food and Biological Engineering, Chengdu University, 2025 Chengluo Avenue, Chengdu, 610106, China
[b] College of Food and Biological Engineering, Henan University of Animal Husbandry and Economy, Zhengzhou, 450046, China

ARTICLE INFO

Editor name: Xing Chen

Keywords:
Egg yolk
Low-density lipoprotein
Ultrasound

ABSTRACT

Egg-yolk low-density lipoprotein (LDL) has a natural liposome structure. Using ultrasound-assisted pH-shifting (pH 12), a naturally safe and stable aqueous solution of vitamin D_3 (VD_3) was constructed employing LDL as the carrier. Images from electron microscopy showed that pH-shifting remodeled LDL molecules, resulting in a dramatic reduction in particle size (~50%) and an increase in specific surface area, which reduced the turbidity (27.7%) and provided new interfaces for VD_3 loading. Fluorescence analyses showed that the binding of VD_3 to LDL under pH-shifting was strong, involved quenching, and the binding constant was 6.19×10^4 M^{-1}. Thermogravimetric analysis and Fourier transform-infrared spectroscopy showed that pH-shifting hydrolyzed the esters in LDL to fatty acid salts, and the maximum weight loss of LDL occurred from 381.9 °C to 457.0 °C. Ultrasonic treatment enhanced the binding of LDL and VD_3 (binding constant increased to 2.56×10^7 M^{-1}), reduced the particle size, and increased the ζ-potential of the complex between LDL and VD_3, thereby resulting in the improvement of solution stability and storage stability of VD_3. Ultrasound-assisted pH-shifting could remodel LDL to construct a stable aqueous solution of VD_3, which showed the potential of LDL as a carrier for lipid-soluble components.

1. Introduction

Vitamin D (VD) is a lipophilic compound. It is present in plant foods and animal foods as ergocalciferol (VD_2) and cholecalciferol (VD_3), respectively (Calvo et al., 2013; Tripkovic et al., 2017). VD plays an important part in calcium absorption, healthy bone metabolism, and cancer prevention (Xia et al., 2011). Severe deficiency of VD can cause osteoporosis in adults, or rickets and dysplasia in infants (Gani and How, 2015). Several diseases are strongly associated with VD deficiency, such as allergies, autoimmune diseases, depression, diabetes mellitus, breast cancer, and colorectal cancer (Zhang et al., 2019). VD suppresses autoimmunity and the inflammatory response (Chirumbolo et al., 2017). Recent studies have suggested that VD deficiency may increase the risk of severe acute respiratory syndrome-coronavirus-2 (SARS-CoV-2) infection and severe illness and mortality (Merzon et al., 2020). VD supplementation can improve the prognosis of SARS-CoV-2 infection if it is timely (Castillo et al., 2020). However, VD is present in only some foods, such as oily fish (e.g., salmon), eggs (egg yolk), liver, and mushrooms (Lamsen et al., 2020). Hence, ~30% of children and ~60% of adults worldwide are deficient in VD (Daly et al., 2012), due mainly to insufficient exposure to sunlight and inadequate dietary intake.

Adding extra VD to processed foods is an effective way to reduce deficiencies. VD_3 is one of the most common VD nutritional supplements (Perales et al., 2005). However, as a fat-soluble compound, VD_3 has poor solubility in water, which reduces its stability and bioavailability. Several studies have shown that "nanocapsules" can improve the system stability and bioavailability of fat-soluble compounds. Protein spheres, polysaccharides, and their chemical crosslinkers (Zhou et al., 2018) can be used as nanocapsule carriers. Gum Arabic has been used to encapsulate VD_3 to improve its bioavailability and stability in beverages (Lamsen et al., 2020). Nanocapsules with good performance have been formed using β-lactoglobulin from cress-seed mucilage to encapsulate VD_3 (Taheri et al., 2021), allied with addition of calcium ions to increase the rigidity of the nanocapsules. Nanocapsules with phospholipids as wall materials are usually called "liposomes", which are self-assembled closed vesicles with a phospholipid bilayer (Deshpande et al., 2016). Liposomes have sizes ranging from a few tens of nanometers to a few

* Corresponding author.
E-mail address: gengfang@cdu.edu.cn (F. Geng).
[1] These authors contributed equally to this work.

https://doi.org/10.1016/j.crfs.2022.05.013
Received 23 April 2022; Received in revised form 18 May 2022; Accepted 24 May 2022
Available online 9 June 2022

micrometers (Akhavan et al., 2018). Their bilayers consist of amphiphilic phospholipid molecules with a hydrophobic "tail" and hydrophilic "head", which is the main reason why liposomes can be used as carriers for transporting active substances.

Egg-yolk low-density lipoprotein (LDL) is rich in cholesterol, which has the same "molecular backbone" as VD_3. Therefore, LDL could be an ideal carrier for encapsulated loading of VD_3. LDL has a natural liposome structure of diameter 17–60 nm. The widely accepted structural model of LDL is that lipids (triglycerides and cholesterol) are encapsulated by a phospholipid monolayer, and apoprotein fragments (apolipoprotein B) and part of cholesterol are embedded in the phospholipid monolayer to stabilize the structure (Anton, 2013; Xie et al., 2020a). LDL has the most efficient capacity to transport lipids, and is considered to be a "delivery vehicle" for drugs or the active ingredients in food. However, LDL is like a "truck" full of lipid molecules, and how to load VD_3 onto LDL is a key requirement. One approach is to delipidate LDL partially and then "reload" the target components with the assistance of emulsifiers. Fei and colleagues (Fei et al., 2021) studied partially defatted LDL compounded with carboxymethylcellulose and encapsulated cannabidiol with the help of emulsifiers (Tween-80 and sodium dodecyl sulfate) to form nanocapsules. Partial removal of fat facilitates embedding, but excessive removal leads to aggregation of hydrophobic proteins and leads to instability (Fei et al., 2021; Kudre et al., 2018). Another approach is to modify or allow LDL to form a complex with other macromolecules (e.g., polysaccharides), thereby enhancing its loading capacity. Zhou and coworkers (Zhou et al., 2016) demonstrated that nanogels formed of a complex between LDL and pectin could be used as oral delivery carriers for curcumin. Nanogels prepared by chemical crosslinking of 1-ethyl-3-(3-dimethyl-aminopropyl-1-carbodiimide)/N--hydroxysuccinimide/LDL/polysaccharides could improve the stability of nanogels significantly and increase the encapsulation efficiency (Zhou et al., 2018). However, such methods require use of organic solvents for degreasing or the addition of polysaccharides, thereby adding operational steps and costs.

"pH-shifting" is an environmentally friendly and effective method to change the structure of macromolecules (Fang et al., 2021; Li et al., 2022). Significantly smaller sizes of LDL were found under alkaline conditions (Zhou et al., 2016), the decrease in particle size leads to an increase in specific surface area and surface energy (Csiszár et al., 2013), which could promote the better adsorption of small molecules. Meanwhile, solubility in an alkaline environment has been observed for water-insoluble substances, including VD_3 (Pan et al., 2014). However, it is not sufficient to build an excellent aqueous phase system rely only on pH-shifting. Therefore, ultrasound assistance is considered to enhance the stability of the solution. Previously, we showed that ultrasonic treatment induced structural remodeling and mild aggregation of LDL, so encapsulation of the target active ingredient during aggregation could occur (Xie et al., 2020a). Based on that information, we tried to reconstruct LDL and dissolve VD_3 by ultrasound-assisted pH-shifting. The stable aqueous solution of VD_3 we constructed could expand the application scope of VD_3 in food processing.

2. Materials and methods

2.1. Sample preparation

LDL was prepared from eggs laid by Roman hens (50–60 weeks) eating a standard diet while caged. Eggs were collected from a poultry farm (Mianyang, Sichuan, China) within 72 h of being laid. Egg yolks were separated from fresh eggs, and rolled dry on clean filter paper. Then, the yolk membrane was punctured to obtain yolk. LDL preparation was undertaken according to the method described by Wang and colleagues (Wang et al., 2018) and Xie and coworkers (Xie et al., 2020a).

LDL was dispersed homogeneously in phosphate-buffered saline (PBS; 10 mM; pH 7.2) with a magnetic stirrer (4 °C, 1 h) to form a LDL solution (2 mg/mL). VD_3 (United States Pharmacopeia grade; Sangon Biotech, Shanghai, China) was dissolved in anhydrous ethanol to form a stock solution of VD_3 (10 mg/mL).

Preparation of pH-shifted LDL (pH12-LDL) involved adjustment of the LDL solution (80 mL, 2 mg/mL) to pH 12 using NaOH (4 mol/L).

For preparation of a mixture of LDL and VD_3 (LDL-VD_3), LDL solution (80 mL) was mixed with the stock solution of VD_3 (0.5 mL) and magnetic stirring undertaken at 300 rpm for 30 min in the dark.

For preparation of a mixture of LDL and VD_3 under pH-shifting (pH12-LDL-VD_3), we used LDL solution (80 mL) to adjust the pH to 12 by employing NaOH. Then, 0.5 mL of the stock solution of VD_3 was added to it, followed by magnetic stirring at 300 rpm for 30 min in the dark.

For preparation of a mixture of LDL and VD3 under pH-shiftingand ultrasonic treatment (pH12-LDL-VD_3-U), the pH12-LDL-VD_3 solution (80 mL) was treated by an ultrasonic generator with a 6-mm probe (JY92-IIDN; Ningbo Xinzhi Biotechnology, Ningbo, China) for a total of 10 min (ultrasound for 3 s, stop for 3 s) at a power setting of 200 W (Xie et al., 2020a, 2020b).

2.2. Determination of turbidity, ζ-potential, and particle size

The turbidity of samples was measured by a turbidimeter (WZS-188; Shanghai Yidian Scientific Instruments, Shanghai, China). Zero-turbidity water was prepared according to Chinese Standard GB/T 13200-1991 (distilled water was passed through a membrane of size 0.2 μm) to calibrate the instrument, after which the sample could be tested directly.

Prepared samples were diluted to 0.2 mg/mL with water of the corresponding pH value. The ζ-potential and mean particle size of each group of samples were measured by a nanoparticle sizer (ZS90; Malvern Zetasizer Nano, Malvern, UK) (Huang et al., 2022; Xiong et al., 2021). The measurement temperature was 25 °C and the parameters were set according to the instrument's manual. Three replicate measurements were undertaken for each sample.

2.3. Encapsulation efficiency

The encapsulation efficiency (EE) of pH12-LDL-VD_3 and pH12-LDL-VD_3-U was measured by ultra-filtration centrifugation (Li et al., 2009). Ultra-filtration centrifuge tubes (Inner tube volume: 15 mL, retained molecular weight: 10 KDa; Shanghai Titan Technology Co., Ltd., Shanghai, China). Samples (2 mL) was added into the inner tube to centrifuge (6000×*g*, 10 min) and rinse 3 times by water (pH12) to extract all of the free VD_3. The absorbance of VD_3 at 265 nm were acquired using an UV–vis spectrophotometer (UV1901PC; Shanghai Aoan Scientific Instruments, Shanghai, China).

EE was calculated by the standard curve:

$$EE\ \% = \frac{\text{total VD3} - \text{free VD3}}{\text{total VD3}} \times 100\% \quad (1)$$

2.4. Ultraviolet–visible (UV–vis) spectroscopy

VD_3 degradation was measured in the presence/absence of LDL and with/without ultrasonic treatment. The stock solution of VD_3 (0.5 mL) was mixed with PBS (80 mL, 10 mmol/L) and adjusted to pH 12 with NaOH as the control sample. The control, pH12-LDL-VD_3, and pH12-LDL-VD_3-U samples were stored away from light for 72 h at 25 °C. The absorbance spectra of control, pH12-LDL-VD_3, and pH12-LDL-VD_3-U samples were acquired from 200 nm to 400 nm every 12 h using an UV–vis spectrophotometer (UV1901PC; Shanghai Aoan Scientific Instruments, Shanghai, China). Samples were diluted 5-fold by water (pH = 12) before UV–Vis spectroscopy.

2.5. Fluorescence spectroscopy

VD_3 (5–25 mg/L) was added to pH-shifted LDL solution (2 mg/mL) with or without ultrasonic treatment. The intrinsic fluorescence of samples was measured with a fluorescence spectrophotometer (FL-970; Shanghai Tianmei Scientific Instruments, Shanghai, China). The excitation slit width and emission slit width were 2.5 nm, respectively, and the excitation wavelength was 280 nm. Scanning was carried out at an emission wavelength of 300–500 nm. Fluorescence quenching was analyzed according to the Stern–Volmer equation:

$$F0/F = 1 + Kq \times \tau 0 \times [Q] = 1 + K_{SV} \times [Q] \quad (2)$$

where *F0* and *F* are the maximum fluorescence intensity without and with a quencher, respectively, [Q] is the concentration of VD_3 (mol/L), *Kq* is the fluorescence quenching rate constant, *τ0* is the lifetime of fluorophore fluorescence in the absence of a quencher (10^{-8} s), and *Ksv* is the Stern–Volmer quenching constant. The apparent binding constant (*Ka*) and number of binding sites (*n*) can be calculated using the double-logarithmic Stern–Volmer equation:

$$\log [(F0 - F)]/F] = \log Ka + n \times \log [Q] \quad (3)$$

By plotting log [(*F0* – *F*)/*F*] against log [VD_3], a linear curve is obtained with a slope of *n*. The intercept provides the value of log *Ka* (Wu et al., 2020, 2021).

2.6. Particle morphology

For scanning electron microscopy (SEM), samples were diluted to 0.05 mg/mL with deionized water of the corresponding pH value. Diluted samples (10 μL) were added to clean slides, air-dried for 24 h, and then observed with a scanning electron microscope (Apreo 2C; Thermo Fisher Scientific, Waltham, MA, USA) at an acceleration voltage of 10 kV (Luo et al., 2021; Wang et al., 2022).

For transmission electron microscopy (TEM), samples were diluted to 0.2 mg/mL with deionized water of the corresponding pH value. Diluted samples (10 μL) were added to a copper mesh to dry in air. One small drop of phosphotungstic acid was used for negative dyeing for 30 s. The microstructures of different samples were recorded by a high-resolution transmission electron microscope (HT7700; Hitachi, Tokyo, Japan) at an acceleration voltage of 100 kV (Geng et al., 2021a).

2.7. Thermogravimetric analysis (TGA)

The thermal stability of lyophilized samples (10 mg) was analyzed using a thermal analyzer (STA449F5; Netzsch Instrument Manufacturing, Munich, Germany) under the following parameters: test temperature = 60–750 °C, heating rate = 5 °C/min, carrier gas = high-purity (99.999%) nitrogen, and flow rate of carrier gas = 50 mL/min (Li et al., 2021; Yu et al., 2022a).

2.8. Fourier transform-infrared (FT-IR) spectroscopy

Lyophilized samples (1–2 mg) were mixed fully with dried KBr (100 mg), placed on a plate with ZnSe crystals, and pressed into tablets. Spectra were acquired at 400–4000 cm^{-1} in 32 scans at a resolution of 4 cm^{-1} using an attenuated total reflection-FTIR spectrometer (Thermo Fisher Scientific) (Yu et al., 2022b).

2.9. Statistical analyses

Data are the mean with standard deviation. Statistical analyses were undertaken using Prism 8 (GraphPad, La Jolla, CA, USA) by one-way analysis of variance, and $p < 0.05$ were considered significant.

3. Results

3.1. Properties of an aqueous solution of VD_3

The turbidity and particle size of LDL solution (2 mg/mL, pH 7.2, PBS) was 39.16 NTU and 100.80 ± 6.74 nm, respectively, which was due mainly to the mild aggregation of LDL in neutral solution (Fig. 1A and B). After VD_3 addition, the turbidity of LDL-VD_3 solution increased by 495.04% compared with the turbidity of the LDL solution, and the particle size increased to 269.78 ± 50.69 nm. These results suggested VD_3 deposition and potential aggregation between insoluble VD_3 particles and LDL. The LDL-VD_3 solution exhibited poor stability and significant precipitation after 1 week of storage (Fig. S1). Compared with the LDL solution, the pH-shifted LDL (pH12-LDL) solution became clear, turbidity dropped to 28.32 NTU, and the particle size decreased to 51.59 nm. These changes were due to the strong intermolecular repulsion and hydrophobic interactions in alkaline solution, and suggested that pH-shifting changed the structure of LDL significantly. In contrast to LDL-VD_3, the turbidity of pH12-LDL-VD_3 solution dropped significantly to 73.09%, and the size of particles in the solution decreased by 57.67%. The pH12-LDL-VD3 solution exhibited better stability and no significant precipitation after 2 weeks of storage (Fig. S1). Hence, pH-shifting could improve solution stability significantly, possibly through "remodeling" of LDL molecules.

The ζ-potential of LDL solution was −4.11 ± 0.30 mV, and VD_3 addition enhanced it to −6.48 ± 0.69 mV (Fig. 1C). In contrast, the ζ-potential of pH12-LDL (−20.54 ± 2.01 mV) and pH12-LDL-VD3 (−23.91 ± 3.08 mV) was enhanced significantly under pH-shifting. The stronger electrostatic repulsion caused by the enhanced ζ-potential could be one of the reasons why pH-shifted solutions were more stable. After ultrasonic treatment, the size of particles in pH12-LDL-VD3-U decreased by 26.53% and the ζ-potential increased by 7.19% compared with those in pH12-LDL-VD3, and the turbidity decreased to 42.12 NTU. These results indicated that the cavitation effect produced by ultrasonic treatment further changed the structure of LDL, or altered the binding of LDL to VD3.

In conclusion, pH-shifting greatly improved the solubility and solution stability of aqueous LDL-VD_3 mainly by reducing the particle size and enhancing the surface potential of LDL-VD3. These changes suggested that pH-shifting remodeled the molecular structure of LDL. In addition, ultrasonic treatment could further enhance the stability of an aqueous solution of LDL-VD_3.

3.2. Storage stability of an aqueous solution of VD_3

Although pH-shifting and ultrasonic treatment improved the aqueous-phase dissolution and solution stability of VD_3, we needed to ascertain if VD_3 would degrade under the combined treatment of pH-shifting and sonication. The UV absorption of VD_3 at 265 nm can be used to monitor its content changes in aqueous solutions. Therefore, the UV spectra of samples were recorded and compared during storage (0–72 h). We discovered that the UV absorption of VD_3 (pH 12, in PBS) was degraded by 71.82% after storage for 72 h (Fig. 2A), which suggested that VD_3 was degraded rapidly in PBS under pH-shifting. In the presence of LDL, VD_3 degradation was delayed substantially: the drop in UV absorption of pH12-LDL-VD_3 was only 22.42% after storage for 72 h (Fig. 2B). After ultrasonic treatment, the storage stability of an aqueous solution of VD3 (pH12-LDL-VD_3-U) was improved further (Fig. 2C).

These results suggested that LDL provided good protection and inhibited VD_3 degradation under pH-shifting and ultrasonic treatments. The protective effect of LDL on VD_3 may have been due to molecular remodeling under pH-shifting exposing many hydrophobic surfaces, thereby providing interfaces for VD_3 loading. VD_3 may also have been loaded by binding to LDL surface-embedded protein fragments. Binding to LDL limits the freedom of the VD_3 molecule and inhibits its potential reaction with oxygen, thereby improving its stability in aqueous

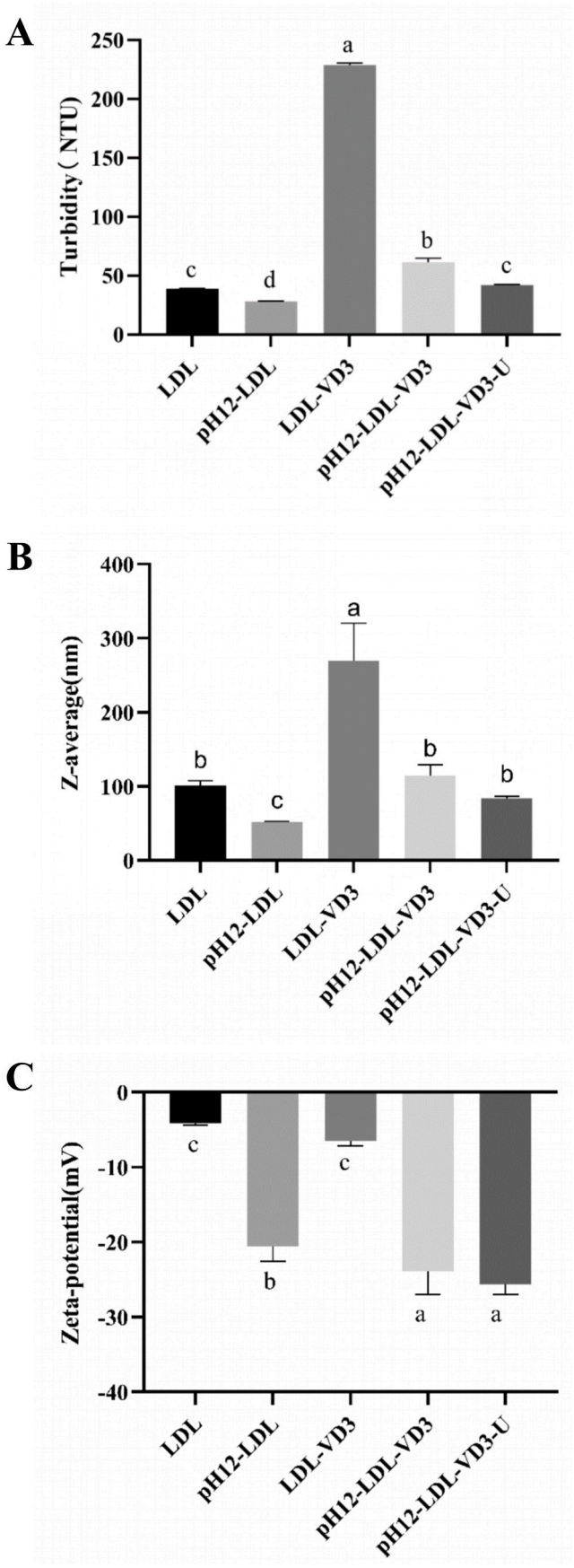

Fig. 1. Turbidity (a), particle size (b), and ζ-potential (c) of LDL, pH12-LDL, LDL-VD_3, pH12-LDL-VD_3, and pH12-LDL-VD_3-U.

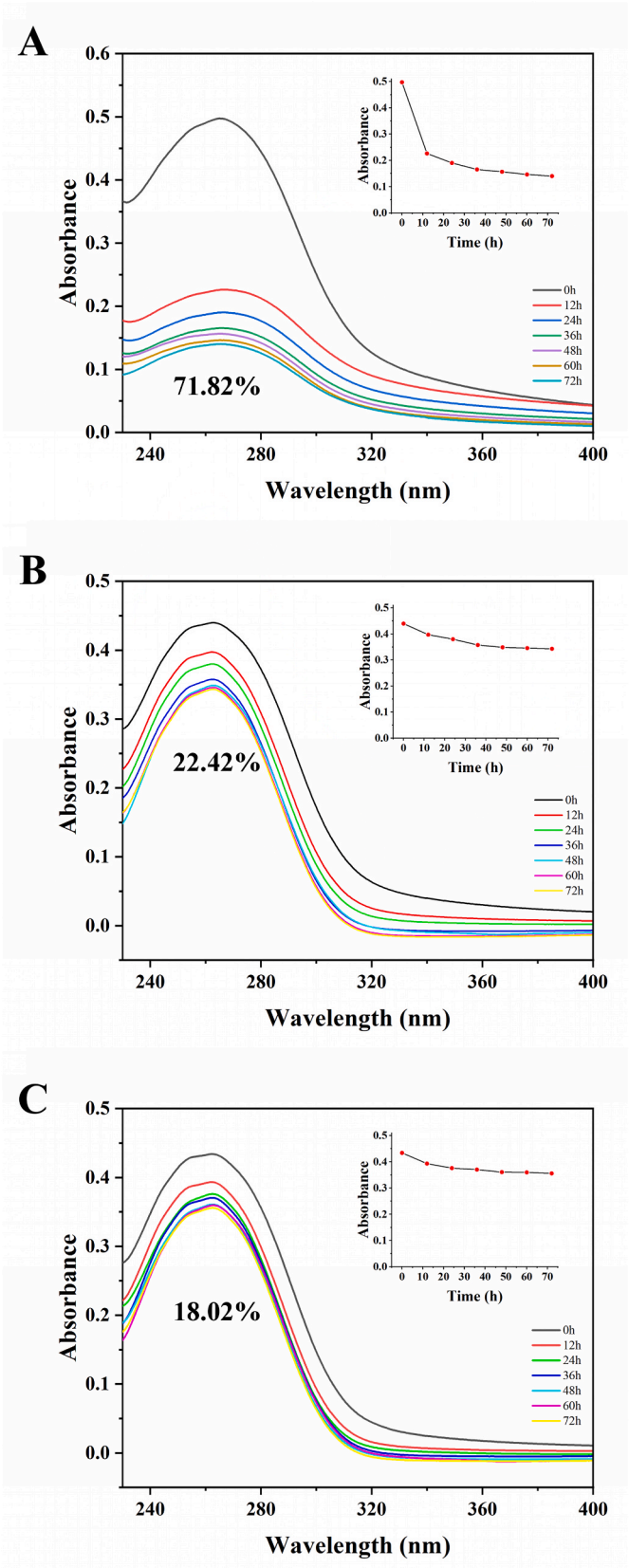

Fig. 2. UV absorbance spectra of pH12-PBS-VD3 (a), pH12-LDL-VD3 (b), and pH12-LDL-VD3-U (c). Insert: linear plot of absorbance *vs.* storage time using the change in maximum intensity of UV absorbance.

solutions greatly. Ultrasonic treatment improved the stability of VD_3 solution further possibly by enhancing the binding between LDL and VD_3. Microstructural observations, interaction analyses, thermodynamic measurements, and spectroscopy were undertaken to provide evidence to confirm these speculations.

3.3. Microstructure

TEM images showed that untreated LDL molecules were regular spheres with clear boundaries, and the size range was 50–200 nm (Fig. 3A), which was consistent with the results of particle-size analyses (Fig. 1B) and our previous results [16]. Adhesion between LDL molecules was observed on SEM images (Fig. 3B), which may have been caused by dehydration treatment before SEM observation. After pH-shifting, most pH12-LDL molecules were reduced to size 20–30 nm, with a small proportion of size 50–100 nm (Fig. 3C), which confirmed directly that pH-shifting reduced the particle size of LDL. Images of LDL-VD3 showed many irregular shapes of size >200 nm (Fig. 3E) and extensive adhesion/aggregation (Fig. 3F). These morphologies were consistent with a significantly increased particle size and turbidity of LDL-VD3, and suggested that direct mixing of VD_3 with LDL was not conducive to dissolution of the aqueous phase and solution stability of VD_3. Addition of VD_3 to pH-shifted LDL solution resulted in uniform, spherical pH12-LDL-VD3 particles of size 30–50 nm (Fig. 3G). After ultrasonic treatment, the pH12-LDL-VD3-U sample was disaggregated mostly to 10–20 nm, but a small amount of the sample contained aggregated particles of size 100 nm (Fig. 3I). TEM and SEM images provided direct evidence of pH-shifting causing remodeling of LDL molecules.

3.4. Interaction between LDL and VD_3

Quenching of LDL fluorescent chromophores after VD_3 addition was measured to characterize the binding properties between LDL and VD_3. The fluorescence spectra of pH-shifted LDL solution (pH 12, 2 mg/mL) in the presence of different concentrations of VD_3 are shown in Fig. 4A. LDL exhibited a strong fluorescence emission peak at 328–332 nm. The fluorescence intensity of LDL decreased markedly upon VD_3 addition.

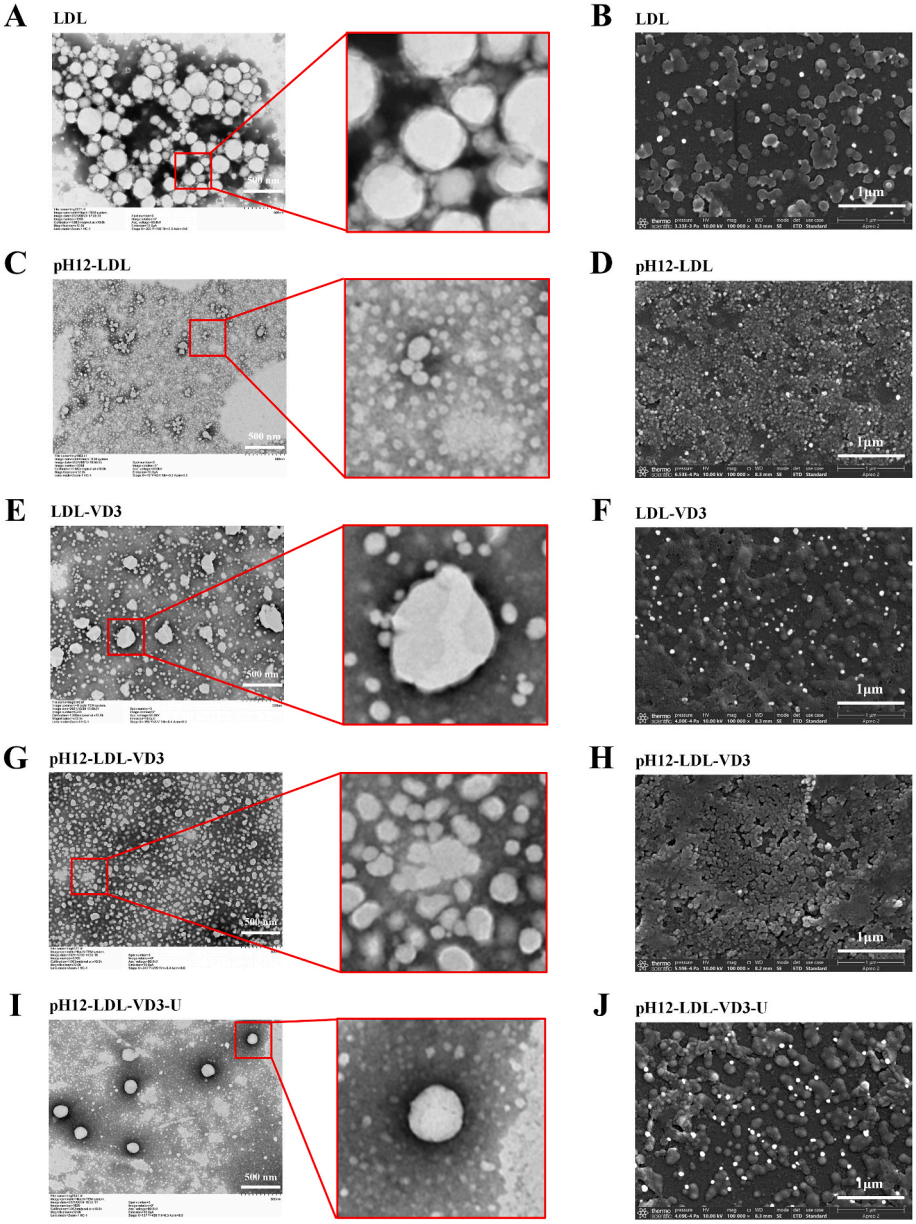

Fig. 3. Morphology of LDL (A/B), pH12-LDL (C/D), LDL-VD3 (E/F), pH12-LDL-VD3 (G/H), and pH12-LDL-VD3-U (I/J).

After ultrasonic treatment, the quenching of LDL fluorescent chromophores after VD_3 addition was also observed but with a steeper slope (Fig. 4B). Fluorescence-quenching data were analyzed, and *Kq* was calculated based on Equation 2. *Kq* with ($0.42–1.5 \times 10^{12}$) or without ($1.04–1.39 \times 10^{12}$) ultrasonic treatment was greater than the collision quenching constant (2×10^{10} L/(M^{-1} s^{-1})), which suggested that the quenching mechanism between VD_3 and LDL was complex formation (static) instead of a collision (dynamic).

For static quenching, the complex-forming phenomena between VD_3 and LDL could be delineated using Equation (3). Plots of log(*F0 – F*)/*F* against log [*Q*] are shown in Fig. 4C. The *n* value (slope) was 1.161, indicating a binding stoichiometry of approximately 1:1 for the interaction between LDL and VD_3 under pH-shifting. Upon ultrasonic treatment, the binding stoichiometry of the interaction between LDL and VD_3 increased to 1.768. The value of the binding constant *Ka* (intercept) of LDL to VD_3 under pH-shifting was 6.19×10^4 M^{-1}, and increased substantially to 2.56×10^7 after ultrasonic treatment. The increased values of *n* and *Ka* suggested that ultrasonic treatment increased the binding capacity and affinity of LDL to VD_3, which was consistent with the observed phenomenon: pH12-LDL-VD3-U had lower turbidity (Fig. 1A), smaller particle size (Fig. 1B), and lower degradation rate (Fig. 2C) than those of pH12-LDL-VD3. Similar results were also obtained by the EE measurement, with pH12-LDL-VD3-U (90.74%) having a significantly high EE compared to pH12-LDL-VD3 (85.63%). Which showed that the assistance of ultrasound treatment promoted the binding of LDL to VD_3. The results of interaction analyses confirmed the high affinity of VD3 to the LDL-protein fraction.

3.5. Thermal stability

Thermal properties could reflect the influence of pH-shifting and ultrasonic treatment on LDL and the LDL-VD3 complex. The TGA curve showed that the mass loss of VD_3 accelerated above 250 °C, and the maximum rate of mass loss was at 350.6 °C (Fig. 5A). LDL had a small mass loss (~2%) below 280 °C, and its derivative thermogravimetric (DTG) curve had a weak peak at 249.0 °C; the main mass loss was between 280 °C and 400 °C, and the DTG peak was at 381.9 °C (Fig. 5B and C). The residual mass (~86%) was salts (sodium chloride and phosphates) after lyophilization of LDL solution. After pH-shifting, the thermal stability of pH12-LDL changed significantly: ~5% of its mass was lost from room temperature to 350 °C, and the DTG curve had two peaks, at 179.0 °C and 246.2 °C, respectively; the mass loss of the second stage was ~6% in the range 350–500 °C. The TGA and DTG curves of LDL-VD3 were similar to that of LDL, which suggested that direct mixing of VD_3 with LDL did not alter thermal stability. The TGA/DTG curves of pH12-LDL-VD3 and pH12-LDL had some differences in the range from room temperature to 350 °C: the weight loss was higher (~7.5%) due to VD_3 addition, and the peak of the DTG curve changed to 299.2 °C. The TGA/DTG curves of pH12-LDL-VD3 and pH12-LDL-VD3-U were almost identical, indicating that the thermal stability of samples was not altered by ultrasonic treatment. These changes in thermal stability of samples suggested that, in addition to the remodeling effects on LDL molecules, pH-shifting might induce changes in LDL composition (e.g., saponification of lipids in the alkaline solution and the resulting increase in free fatty acids and sodium salts of fatty acids).

3.6. FT-IR spectroscopy

The FT-IR spectra of LDL and pH12-LDL were compared to ascertain if pH-shifting changed the material composition. The FT-IR spectrum of LDL and pH12-LDL had the same absorption peaks (in cm^{-1}) at 1653–1658, 2852–2854 and 2922–2924, which corresponded to the amide-I band (protein part of LDL), symmetric stretching vibrations of the CH_2 group, and asymmetric stretching vibrations of the CH_2 group, respectively (Fig. 6) (Krilov et al., 2009). In addition to these absorption peaks, the other main absorption peaks of the pH12-LDL sample were

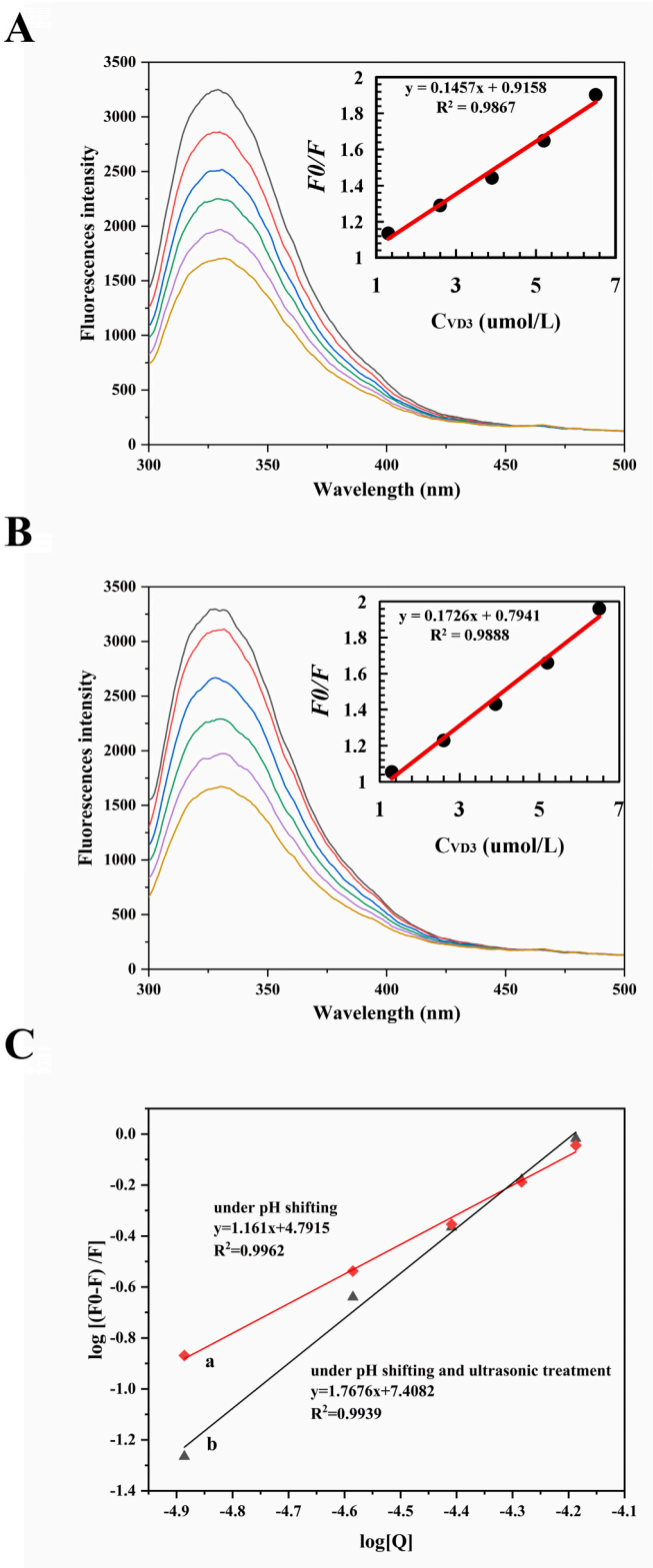

Fig. 4. Fluorescence spectra of pH12-LDL-VD3 (a) and pH12-LDL-VD3-U (b) with different VD3 concentrations. Insert: linear plot of F0/F *vs.* C(VD3) using the change in the maximum fluorescence intensity of pH12-LDL-VD3 and pH12-LDL-VD3-U. Linear plot of log[(F0 − F)/F] *vs.* log[C(VD3)] (c).

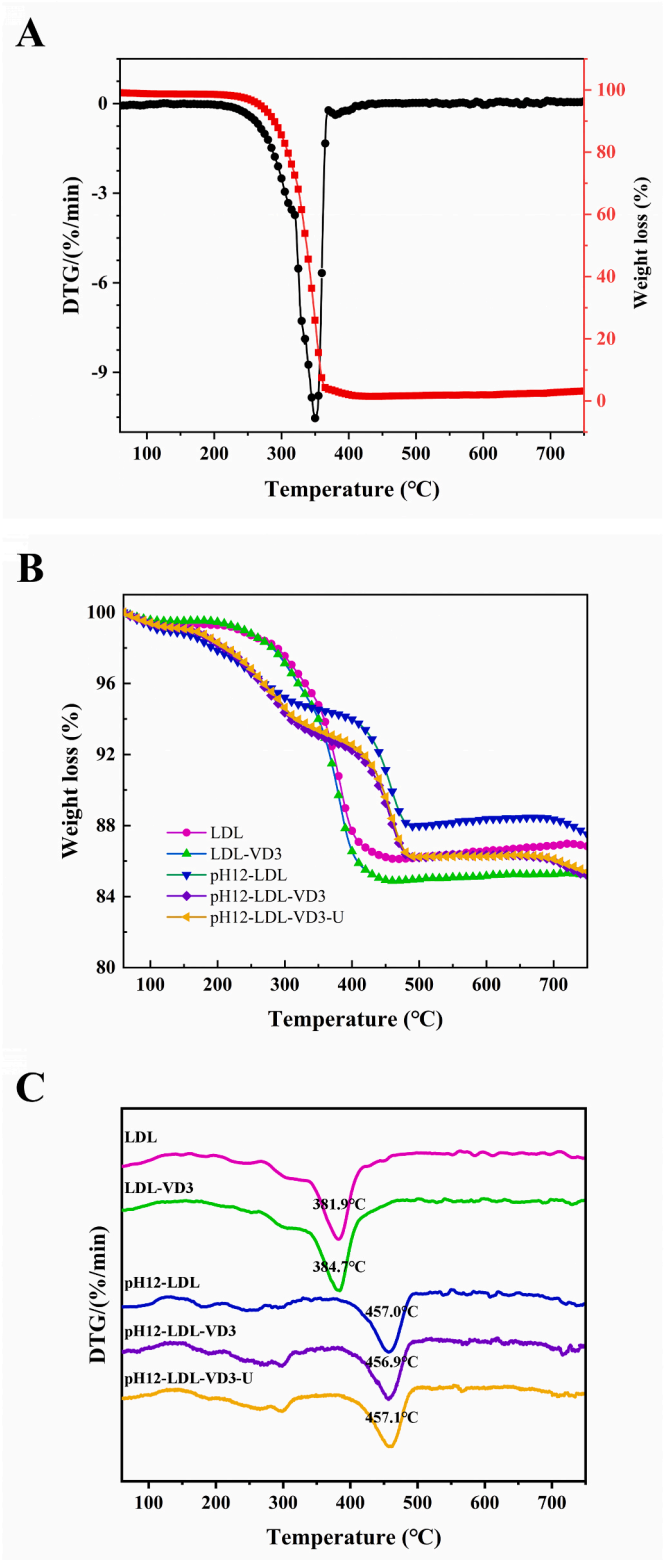

Fig. 5. TGA and DTG curves of VD3 (a), TGA (b) and DTG (c) curves of LDL, pH12-LDL, LDL-VD3, pH12-LDL-VD3, and pH12-LDL-VD3-U.

changed. On the FT-IR spectrum of LDL, the absorption peak of the C=O stretching vibration at 1744 cm^{-1} (Zhou et al., 2018), and the double absorption peaks of the C–O–C stretching vibration at 1090 cm^{-1} and 1150 cm^{-1} were the characteristic absorption peaks of esters. These peaks were missing in the FT-IR spectrum of the pH12-LDL sample. Correspondingly, the characteristic absorption peaks of carboxylic acid

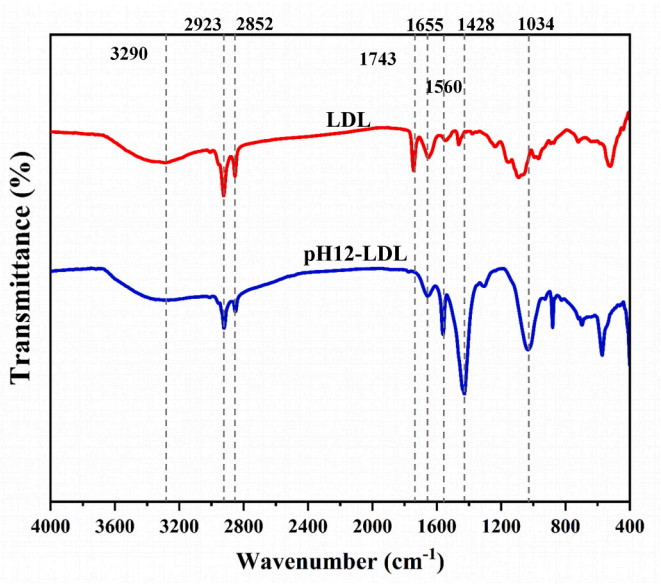

Fig. 6. FTIR spectra of LDL and pH12-LDL.

were observed in the spectrum of the pH12-LDL sample: the OH out-of-plane bending vibration at 879 cm^{-1}, and the COO symmetrical stretching vibration at 1428 cm^{-1}. These changes suggested that the lipids in the LDL molecule were hydrolyzed to fatty acids under pH-shifting.

4. Discussion

4.1. pH-shifting remodels LDL

SEM and TEM images provided key evidence that pH-shifting remodeled the LDL molecule. However, the results of microstructural observations were not completely consistent with those of particle-size analyses of solutions. SEM and TEM showed that LDL was depolymerized into smaller particles under pH-shifting, and that the particle size was reduced by ~5-fold (Fig. 3A and C). Particle-size analyses of solutions showed that the particle size of pH12-LDL decreased by 48.82% (Fig. 1B). This difference may be have been due to the dramatic increase in the specific surface area caused by the depolymerization of LDL molecules by pH-shifting. This action exposes the lipid core, and large areas of lipid surfaces not covered by the phospholipid monolayer tend to adhere to each other. This feature could be observed by SEM. The adhesion between depolymerized LDL resulted in a larger mean particle size when analyzing the particle size of pH12-LDL in solution using dynamic light scattering. In addition, a substantial reduction in turbidity (less scattering of light) was important evidence that LDL molecules were depolymerized under pH-shifting.

In addition to causing the depolymerization of LDL, pH-shifting led to other important changes. An obvious change was that lipids in LDL molecules were hydrolyzed to sodium salts of fatty acids under alkaline conditions, which was confirmed by FT-IR spectroscopy. In addition, TGA curves showed a sustained mass loss in the range from room temperature to 350 °C, which corresponded to the thermal degradation of fatty acids induced by pH-shifting. The changes in the DTG curve of LDL after pH-shifting were consistent with those reported previously, in which the DTG curves of soybean oil and oleic acid changed from a single peak to multiple peaks after CaO addition, and showed a more complex process of thermal degradation (Zhang et al., 2014). Sodium salts of fatty acids are amphiphilic molecules that can be adsorbed rapidly to the surface of LDL molecules after being cleaved by pH-shifting. This action should be the main reason why pH12-LDL could remain stable without large-scale aggregation despite the dramatic

increase in specific surface area. In addition, pH shifting-induced remodeling enhanced the thermal stability of approximately half of LDL components, and DTG curves exhibited mass-loss stages in a higher temperature range, with a maximum rate of mass loss at 457 °C.

The LDL molecule was fully remodeled through pH-shifting. Its particle size was reduced, and its specific surface area was increased. This strategy provides an important premise for using LDL to load active ingredients in food. In addition, pH-shifting is much safer, simpler, and cheaper than defatting or adding polysaccharides (Fei et al., 2021; Kudre et al., 2018; Zhou et al., 2016, 2018). Therefore, pH-shifting-induced remodeling of LDL molecules can be used as a general processing method to load/encapsulate active ingredients, and has broad and competitive application potential.

4.2. VD_3 binds to remodeled LDL

Direct mixing of VD_3 with LDL resulted in a several-fold increase in particle size and turbidity (Fig. 1A and B), instability of the solution system, and production of flocculent suspensions after storage (Fig. S1). TEM images revealed the instability caused by direct mixing: irregularly shaped large-sized particles were generated (Fig. 3E). Under pH-shifting, the remodeled LDL and VD_3 reassembled into regular-shaped particles, which were observed on TEM images (Fig. 3G), and confirmed by measuring the turbidity (Fig. 1A) and particle size (Fig. 1B) of solutions. The assembly of remodeled LDL with VD_3 was through tight binding, which was confirmed and supported by the calculated binding constant (*Ka* of LDL to VD_3) based on fluorescence quenching. The binding and assembly between LDL and VD_3 induced by pH-shifting led to the stable dissolution of VD_3 in aqueous solution and improved its stability greatly (Fig. 2B).

It should be noted that the binding constant (*Ka*) and binding ratio (*n*) calculated based on fluorescence quenching analysis could only reflect the binding of VD_3 to the protein fraction of LDL, which only accounts for about 12% of the LDL. On the surface of the LDL, the coverage of the phospholipid monolayer is greater than that of the protein fraction. Furthermore, under pH shifting, more surface vacancies were induced due to the large increase in the surface area of LDL. In this case, the lipophilic VD_3 binds more to the lipid fraction on the LDL surface, and this binding cannot be measured in assays based on intrinsic fluorescence of LDL protein fraction. Therefore, the calculated *Ka* and *n* in this study is much smaller than the actual ones. These underestimation of *Ka* and *n* between LDL and VD_3 by fluorescence quenching assay should be paid attention to in the subsequent research and product development.

4.3. Ultrasonic treatment enhanced the stability of the VD_3 aqueous solution

pH12-LDL-VD3-U prepared by combined treatment of pH-shifting and ultrasound showed lower turbidity, smaller particle size, and stronger ζ-potential compared with those of pH12-LDL-VD3 (Fig. 1). The changes induced by ultrasonic treatment were very beneficial to the stability of VD_3 aqueous solution, and further inhibited VD_3 degradation during storage, and resulted in the best storage stability (Fig. 2C). Particle-size analyses showed that ultrasonic treatment reduced the mean particle size of pH12-LDL-VD3-U solution, but some large aggregates were observed under TEM (Fig. 3I). This observation suggested that ultrasound-induced depolymerization and aggregation might occur simultaneously. This heterogeneity in sonication was also observed by Geng and colleagues: ultrasound induced depolymerization of yolk granules at low and medium power (90–270 W), but reaggregation at 360 W (Geng et al., 2021b). The improved stability of the VD_3 aqueous solution may have been because ultrasonic treatment enhanced the binding of LDL and VD_3 (Fig. 4C). Often, ultrasound is used to promote intermolecular interactions. For instance, ultrasound can promote alkene–aldehyde binding into the interior cavity sites of β-lactoglobulin (Xu et al., 2022). Ultrasound has been shown to induce conformational variations of duck-liver globular proteins and enhance their binding and adsorption to aromatic alkenal substances markedly (Xu et al., 2021).

In summary, a stable aqueous VD_3 solution was constructed by ultrasound-assisted pH shifting and utilizing egg yolk LDL as carriers. In addition to greatly expanding the application range of VD_3 as a nutritional fortifier, the stable aqueous solution may also have potential benefits for the bioavailability of VD_3. First, the structure of LDL is similar to that of liposomes. Therefore, VD_3 bound by LDL was expected to resist the decomposition and destruction under extreme conditions of gastric acid, and reduce the formation of insoluble components with other food components (Liu et al., 2020; Maldonado-Valderrama et al., 2011). Consequently, the VD_3 aqueous solution could reach the small intestine with less loss, which has important benefits for improving the bioavailability of VD_3. In addition, in the small intestine, dietary lipid hydrolysates need to assemble with bile acids, etc., to form spherical micromicelles that cross the hydrostatic barrier to the surface of intestinal epithelial cells (Liu et al., 2012; Tian et al., 2019). Coincidentally, the assembled structure of egg yolk LDL is itself a hydrophilic micromicelle, although there is no conclusive evidence, it is theoretically possible that yolk LDL could effectively cross the hydrostatic barrier and and be absorbed rapidly by intestinal epithelial cells. Therefore, the focus of follow-up research work is to systematically evaluate the effects of the aqueous system constructed in this study on the bioaccessibility of VD_3.

5. Conclusions

pH-shifting remodeled LDL molecules. This action resulted in a reduction in particle size and an increase in specific surface area, which reduced the turbidity. Meanwhile, pH-shifting hydrolyzed the esters in LDL to fatty acid salts and changed its thermal stability and infrared spectra. Under pH-shifting, VD_3 was bound stably to LDL with strong affinity ($6.19 \times 10^4\ M^{-1}$), which resulted in the stable dissolution of VD_3 in aqueous solution and improvement in storage stability. The binding of VD_3 to LDL was enhanced by ultrasonic treatment, and was accompanied by improvements in solution stability and storage stability. Ultrasound-assisted pH-shifting could remodel LDL to construct a stable aqueous solution of VD_3, which showed the potential of LDL as a carrier for lipid-soluble components.

CRediT authorship contribution statement

Haolong Ye: Formal analysis, Methodology, Writing – original draft. **Jinqiu Wang:** Supervision, Writing – original draft, Writing – review & editing. **Ning Wang:** Investigation, Methodology. **Di Wu:** Methodology, Resources. **Hanmei Li:** Data curation, Resources. **Fang Geng:** Conceptualization, Supervision, Writing – original draft, Writing – review & editing.

Declaration of competing interest

The authors declare that they have no known competing financial interests or personal relationships that could have appeared to influence the work reported in this paper.

Acknowledgments

This research was supported by the National Natural Science Foundation of China (32072236).

Appendix A. Supplementary data

Supplementary data to this article can be found online at https://doi.org/10.1016/j.crfs.2022.05.013.

References

Akhavan, S., Assadpour, E., Katouzian, I., Jafari, S.M., 2018. Lipid nano scale cargos for the protection and delivery of food bioactive ingredients and nutraceuticals. Trends Food Sci. Technol. 74, 132–146.

Anton, M., 2013. Egg yolk: structures, functionalities and processes. J. Sci. Food Agric. 93 (12), 2871–2880.

Calvo, M.S., Babu, U.S., Garthoff, L.H., Woods, T.O., Dreher, M., Hill, G., Nagaraja, S., 2013. Vitamin D2 from light-exposed edible mushrooms is safe, bioavailable and effectively supports bone growth in rats. Osteoporos. Int. 24 (1), 197–207.

Castillo, M.E., Costa, L.M.E., Barrios, J.M.V., Diaz, J.F.A., Miranda, J.L., Bouillon, R., Gomez, J.M.Q., 2020. Effect of calcifediol treatment and best available therapy versus best available therapy on intensive care unit admission and mortality among patients hospitalized for COVID-19: a pilot randomized clinical study. J. Steroid Biochem. 203, 105751.

Chirumbolo, S., Bjorklund, G., Sboarina, A., Vella, A., 2017. The role of vitamin D in the immune system as a pro-survival molecule. Clin. Therapeut. 39 (5), 894–916.

Csiszár, E., Fekete, E., Tóth, A., Bandi, É., Koczka, B., Sajó, I., 2013. Effect of particle size on the surface properties and morphology of ground flax. Carbohydr. Polym. 94 (2), 927–933.

Daly, R.M., Gagnon, C., Lu, Z.X., Magliano, D.J., Dunstan, D.W., Sikaris, K.A., Zimmet, P. Z., Ebeling, P.R., Shaw, J.E., 2012. Prevalence of vitamin D deficiency and its determinants in Australian adults aged 25 years and older: a national, population-based study. Clin. Endocrinol (Oxf). 77 (1), 26–35.

Deshpande, S., Caspi, Y., Meijering, A.E., Dekker, C., 2016. Octanol-assisted liposome assembly on chip. Nat. Commun. 7, 10447.

Fang, Z., Cai, X., Wu, J., Zhang, L., Fang, Y., Wang, S., 2021. Effect of simultaneous treatment combining ultrasonication and pH-shifting on SPI in the formation of nanoparticles and encapsulating resveratrol. Food Hydrocolloids 111, 106250.

Fei, T., Wan, Z.F., Wang, T., 2021. Dispersing insoluble yolk low-density lipoprotein (LDL) recovered by complexing with carboxymethylcellulose (CMC) for the nanoencapsulation of hemp cannabidiol (CBD) through emulsification at neutral pH. Food Hydrocolloids 116, 106656.

Gani, L.U., How, C.H., 2015. Vitamin D deficiency. Singap. Med. J. 56 (8), 433–436.

Geng, F., Wen, X., Xu, Y., Zhang, M., Zhou, L., Liu, D., Li, X., Wang, J., 2021a. Phosphoinositide signaling plays a key role in the regulation of cell wall reconstruction during the postharvest morphological development of Dictyophora indusiata. Food Chem. 346, 128890.

Geng, F., Xie, Y., Wang, Y., Wang, J., 2021b. Depolymerization of chicken egg yolk granules induced by high-intensity ultrasound. Food Chem. 354, 129580.

Huang, Q., Liu, L., Wu, Y., Huang, X., Wang, G., Song, H., Geng, F., Luo, P., 2022. Mechanism of differences in characteristics of thick/thin egg whites during storage: physicochemical, functional and molecular structure characteristics analysis. Food Chem. 369, 130828.

Krilov, D., Balarin, M., Kosović, M., Gamulin, O., Brnjas-Kraljević, J., 2009. FT-IR spectroscopy of lipoproteins–a comparative study. Spectrochim. Acta Mol. Biomol. Spectrosc. 73 (4), 701–706.

Kudre, T.G., Bejjanki, S.K., Kanwate, B.W., Sakhare, P.Z., 2018. Comparative study on physicochemical and functional properties of egg powders from Japanese quail and white Leghorn chicken. Int. J. Food Prop. 21 (1), 956–971.

Lamsen, M.R.L., Wang, T., D'Souza, D., Dia, V., Chen, G., Zhong, Q., 2020. Encapsulation of vitamin D(3) in gum Arabic to enhance bioavailability and stability for beverage applications. J. Food Sci. 85 (8), 2368–2379.

Li, H., Zhang, X., Zhao, C., Zhang, H., Chi, Y., Wang, L., Zhang, H., Bai, S., Zhang, X., 2022. Entrapment of curcumin in soy protein isolate using the pH-driven method: nanoencapsulation and formation mechanism. Lebensm. Wiss. Technol. 153, 112480.

Li, J., Ye, J., Sun, T., Kang, L., 2009. Hollow-fiber ultrafiltration then centrifugation for LC analysis of water-soluble sucrose in a water-soluble high-molecular-mass gel matrix. Chromatographia 70, 1023–1030.

Li, S., Wang, K., Huang, Q., Geng, F., 2021. Microwave pretreatment enhanced the properties of ovalbumin-inulin-oil emulsion gels and improved the storage stability of pomegranate seed oil. Food Hydrocolloids 113, 106548.

Liu, W., Hou, Y., Jin, Y., Wang, Y., Xu, X., Han, J., 2020. Research progress on liposomes: application in food, digestion behavior and absorption mechanism. Trends Food Sci. Technol. 104, 177–189.

Liu, W., Ye, A., Liu, C., Liu, W., Singh, H., 2012. Structure and integrity of liposomes prepared from milk- or soybean-derived phospholipids during in vitro digestion. Food Res. Int. 48 (2), 499–506.

Luo, W., Wang, J., Wang, Y., Tang, J., Ren, Y., Geng, F., 2021. Bacteriostatic effects of high-intensity ultrasonic treatment on Bacillus subtilis vegetative cells. Ultrason. Sonochem. 81, 105862.

Maldonado-Valderrama, J., Wilde, P., Macierzanka, A., Mackie, A., 2011. The role of bile salts in digestion. Adv. Colloid Interface Sci. 165 (1), 36–46.

Merzon, E., Tworowski, D., Gorohovski, A., Vinker, S., Cohen, A.G., Green, I., Frenkel-Morgenstern, M., 2020. Low plasma 25(OH) vitamin D level is associated with increased risk of COVID-19 infection: an Israeli population-based study. FEBS J. 287 (17), 3693–3702.

Pan, K., Luo, Y., Gan, Y., Baek, S.J., Zhong, Q., 2014. pH-driven encapsulation of curcumin in self-assembled casein nanoparticles for enhanced dispersibility and bioactivity. Soft Matter 10 (35), 6820–6830.

Perales, S., Alegría, A., Barberá, R., Farré, R., 2005. Review: determination of vitamin D in dairy products by high performance liquid chromatography. Food. Sci. Technol. In 11, 451–462.

Taheri, A., Kashaninejad, M., Tamaddon, A.M., Jafari, S.M., 2021. Vitamin D3 cress seed mucilage-beta-lactoglobulin nanocomplexes: synthesis, characterization, encapsulation and simulated intestinal fluid in vitro release. Carbohydr. Polym. 256, 117420.

Tian, M., Han, J., Ye, A., Liu, W., Xu, X., Yao, Y., Li, K., Kong, Y., Wei, F., Zhou, W., 2019. Structural characterization and biological fate of lactoferrin-loaded liposomes during simulated infant digestion. J. Sci. Food Agric. 99 (6), 2677–2684.

Tripkovic, L., Wilson, L.R., Hart, K., Johnsen, S., de Lusignan, S., Smith, C.P., Bucca, G., Penson, S., Chope, G., Elliott, R., Hyppönen, E., Berry, J.L., Lanham-New, S.A., 2017. Daily supplementation with 15 μg vitamin D(2) compared with vitamin D(3) to increase wintertime 25-hydroxyvitamin D status in healthy South Asian and white European women: a 12-wk randomized, placebo-controlled food-fortification trial. Am. J. Clin. Nutr. 106 (2), 481–490.

Wang, N., Xu, Q., Liu, Y., Jin, Y., Harlina, P.W., Ma, M., 2018. Highly efficient extraction and purification of low-density lipoprotein from hen egg yolk. Poultry Sci. 97 (6), 2230–2238.

Wang, Y., Wang, J., Shi, Y., Ye, H., Luo, W., Geng, F., 2022. Quantitative proteomic analyses during formation of chicken egg yolk. Food Chem. 374, 131828.

Wu, D., Mei, S., Duan, R., Geng, F., Wu, W., Li, X., Cheng, L., Wang, C., 2020. How black tea pigment theaflavin dyes chicken eggs: binding affinity study of theaflavin with ovalbumin. Food Chem. 303, 125407.

Wu, D., Tang, L., Duan, R., Hu, X., Geng, F., Zhang, Y., Peng, L., Li, H., 2021. Interaction mechanisms and structure-affinity relationships between hyperoside and soybean β-conglycinin and glycinin. Food Chem. 347, 129052.

Xia, F., Jin, H.Y., Zhao, Y.P., Guo, X.Q., 2011. Supercritical antisolvent-based Technology for preparation of vitamin D-3 proliposome and its characteristics. Chinese. J. Chem. Eng. 19 (6), 1039–1046.

Xie, Y.X., Wang, J.Q., Shi, Y.N., Wang, Y., Cheng, L., Liu, L.L., Wang, N., Li, H.M., Wu, D., Geng, F., 2020a. Molecular aggregation and property changes of egg yolk low-density lipoprotein induced by ethanol and high-density ultrasound. Ultrason. Sonochem. 63, 104933.

Xie, Y., Wang, J., Wang, Y., Wu, D., Liang, D., Ye, H., Cai, Z., Ma, M., Geng, F., 2020b. Effects of high-intensity ultrasonic (HIU) treatment on the functional properties and assemblage structure of egg yolk. Ultrason. Sonochem. 60, 104767.

Xiong, W., Li, Y., Ren, C., Li, J., Li, B., Geng, F., 2021. Thermodynamic parameters of gelatin-pectin complex coacervation. Food Hydrocolloids 120, 106958.

Xu, L., Zheng, Y., Zhou, C., Pan, D., Geng, F., Cao, J., Xia, Q., 2021. Kinetic response of conformational variation of duck liver globular protein to ultrasonic stimulation and its impact on the binding behavior of n-alkenals. Lebensm. Wiss. Technol. 150, 111890.

Xu, L., Zheng, Y., Zhou, C., Pan, D., Geng, F., Cao, J., Xia, Q., 2022. A structural explanation for enhanced binding behaviors between β-lactoglobulin and alkene-aldehydes upon heat- and ultrasonication-induced protein unfolding. Food Hydrocolloids 130, 107682.

Yu, X., Huang, S., Yang, F., Qin, X., Nie, C., Deng, Q., Huang, F., Xiang, Q., Zhu, Y., Geng, F., 2022a. Effect of microwave exposure to flaxseed on the composition, structure and techno-functionality of gum polysaccharides. Food Hydrocolloids 125, 107447.

Yu, X., Nie, C., Zhao, P., Zhang, H., Qin, X., Deng, Q., Huang, F., Zhu, Y., Geng, F., 2022b. Influences of microwave exposure to flaxseed on the physicochemical stability of oil bodies: implication of interface remodeling. Food Chem. 368, 130802.

Zhang, G., Yu, F., Wang, W., Wang, J., Ji, J., 2014. Influence of molten salts on soybean oil catalytic pyrolysis with/without a basic catalyst. Energy Fuel. 28 (1), 535–541.

Zhang, Y., Fang, F., Tang, J., Jia, L., Feng, Y., Xu, P., Faramand, A., 2019. Association between vitamin D supplementation and mortality: systematic review and meta-analysis. BMJ 366, l4673.

Zhou, M., Khen, K., Wang, T., Hu, Q., Xue, J., Luo, Y., 2018. Chemical crosslinking improves the gastrointestinal stability and enhances nutrient delivery potentials of egg yolk LDL/polysaccharide nanogels. Food Chem. 239, 840–847.

Zhou, M., Wang, T., Hu, Q., Luo, Y., 2016. Low density lipoprotein/pectin complex nanogels as potential oral delivery vehicles for curcumin. Food Hydrocolloids 57, 20–29.